MNRAS **000**, 000–000 (0000) Preprint 22 April 2024 Compiled using MNRAS LATEX style file v3.0

FERMILAB-PUB-24-0183-STUDENT

Cosmic Shear Analysis of the DECam Local Volume Exploration Survey

N. Chicoine★, C. Chang, A. Drlica-Wagner, D. Anbajagane

22 April 2024

ABSTRACT

We forecast cosmological constraints and develop a cosmic shear analysis pipeline for the DECam Local Volume Exploration Survey (DELVE). We test the effects of two different intrinsic alignment frameworks (TATT and NLA) on synthetic data vectors. In addition, we examine the impact of baryon contamination and determine the necessary scale cuts to reduce its influence. We find the forecast results to be as constraining as the DES Y3 cosmological parameter measurements.

1 INTRODUCTION

Despite its simplicity, the standard cosmological model, ΛCDM, proves remarkably powerful. The model consists of a spatially flat universe, guided by general relativity, that contains baryonic matter, dark matter, and a dark energy term that accelerates the Universe's expansion. This model can accurately describe a wide range of observations with only six core parameters, from the structure of the Cosmic Microwave Background (CMB) (Durrer 2015), to the baryon acoustic oscillations (BAO) (Bassett & Hlozek 2010), to strong gravitational cluster lensing (Natarajan et al. 2024). Nonetheless, ΛCDM's success has been tempered by its dependence on two deeply enigmatic components: dark matter and dark energy. In addition, recent experimental results have indicated that the model cannot simultaneously describe the low redshift and high redshift Universe. This project focuses on the so-called S_8 tension. The S_8 parameter characterizes the amplitude of clustering in the large-scale structure of the Universe, defined as $S_8 \equiv \sigma_8\sqrt{\Omega_m/0.3}$. S_8 varies when derived using low-redshift galaxy surveys (Secco et al. 2022; Amon et al. 2022; Asgari et al. 2021; Hikage et al. 2019) vs. high-redshift CMB analysis (Planck Collaboration 2020). Current surveys yield consistently lower S_8 values compared to Planck Collaboration (2020). These inconsistencies demonstrate that we must further test ΛCDM with new measurements to evaluate whether are facing new physics or systematics and precision issues.

Cosmological weak lensing, or cosmic shear, is a powerful and informative low-redshift cosmological probe. When light from a background object passes by the gravitational potential well of a foreground mass or lens, the foreground mass perturbs the source's light and distorts the image. This distortion can occur in terms of both shape and size, or shear and magnification. The larger the lens mass, the deeper the well, and the greater the distortion. Weak gravitational lensing statistically averages the shear of thousands of images of background galaxies to try to extract that distortion. Cosmic shear follows this same principle, but measures the slight distortions of images of distant galaxies caused by the intervening large-scale structure of the Universe. Cosmic shear is particularly sensitive to two cosmological parameters: the total matter density Ω_m and the amplitude of mass fluctuations at a length of 8 Mpc σ_8. As such, cosmic shear is the best probe of the S_8 parameter. This project develops the pipeline for the DECam Local Volume Exploration Survey (DELVE, Drlica-Wagner et al. 2021) cosmic shear analysis and forecasts the cosmological parameter constraints.

2 DATA

DELVE is an optical, near-infrared survey in five different filters *(g,r,i,z,y)* using the Dark Energy Camera (DECam, Flaugher et al. 2015) on the 4-m Blanco Telescope at the Cerro Tololo Inter-American Observatory. The survey aims to understand the characteristics of dwarf satellite galaxies and other stellar substructures across the Local Volume. DELVE will combine archival DECam data from the Dark Energy Survey (DES, Dark Energy Survey Collaboration 2016) with 150 nights of novel observations to cover the entire high-Galactic-latitude southern sky. The new DELVE observations will add 5500 deg^2 of additional coverage and 107 million galaxies to the current DES coverage of 4400 deg^2 and 100 million galaxies. Similar large-scale surveys include the Kilo-Degree Survey (KiDS, de Jong et al. 2013) and the Hyper-Suprime Camera Subaru Strategic Program (HSC SSP, Aihara et al. 2018).

DELVE will leverage existing DES infrastructure to expand the weak lensing analysis to cover 10,000 deg^2 of DECam data, increasing statistical power. The total shear catalog will contain 100 million galaxies and the resulting cosmic shear analysis is predicted to improve constraints on S_8 by 30% compared to DES Year 1 (Abbott et al. 2018).

3 MODEL

3.1 Simulated Data

We briefly overview the construction of synthetic data vectors used to test the modeling process. To construct these data vectors, we first select a baseline cosmology, as listed in Tab 1. We then apply the theoretical model for shear correlation functions (described in Sec. 3.2) to produce a prediction based on this cosmology. The shear correlation model also contains information on the intrinsic alignments, baryon contamination, redshift uncertainty, and other systematics. In essence, the synthetic data vector is merely a prediction of the model. As a consistency check, running the model with only the simulated data vectors will produce posteriors that are consistent with the model inputs.

3.2 Cosmic Shear

We describe the theoretical model for the cosmic shear measurements. Two-point cosmic shear correlations ($\xi_{\pm}^{ij}(\theta)$) are related to the nonlinear matter power spectrum (the gravitationally influenced

Cosmological Parameters	
Ω_m	0.3
h	0.69
Ω_b	0.048
N_s	0.97
w	-1.0
A_s	2.1×10^{-9}
$\Omega_\nu h^2$	0.83×10^{-3}
σ_8	0.82355

Table 1: Initial cosmology used to construct the simulated data vectors.

distribution of matter in the Universe) and the growth and evolution of structure through the convergence κ. κ measures the distortion of a galaxy on a particular line of sight, or the weighted mass overdensity δ integrated along the line-of-sight to the distance of the source χ:

$$\kappa(\theta) = \int_0^{\chi_s} W(\chi)\delta(\theta,\chi)d\chi. \quad (1)$$

The weight, W, of a specific lens plane depends on the relative distances of the source and lens. This geometric term holds the key to using cosmic shear to probe the history of the Universe's expansion. We define the weight as

$$W^i(\chi) = \frac{3H_0^2\Omega_m}{2c^2}\frac{\chi}{a(\chi)}\int_\chi^{\chi_H} n^i(z(\chi'))\frac{\chi'-\chi}{\chi'}\frac{dz}{d\chi'}d\chi'. \quad (2)$$

H_0, Ω_m, $a(\chi)$, $n(z)$, and c refer to the Hubble constant, the matter density of the Universe, the scale factor at the selected line-of-sight distance (or redshift), the redshift distribution, and the speed of light, respectively. In simpler terms, the weight describes the degree of expected lensing that matter at a specific redshift will show. We define the 2D convergence power spectrum in tomographic bins i and j as

$$C_\kappa^{ij}(l) = \int_0^{\chi(z_{\max})} \frac{W^i(\chi)W^j(\chi)}{\chi^2}P_\delta(\frac{l+1/2}{\chi}, z(\chi))d\chi. \quad (3)$$

P_δ represents the nonlinear matter power spectrum. The combination of P_δ and the cosmological terms describes how the matter distribution changes across different directions. We can move from this convergence spectrum (decomposed into E- and B-mode components) to express the angular two-point shear correlations:

$$\xi_\pm^{ij} = \Sigma_l \frac{2l+1}{2\pi l^2(l+1)^2}[G_{l,2}^+(\cos\theta)\pm G_{l,2}^-(\cos\theta)]\times[C_{EE}^{ij}(l)\pm C_{BB}^{ij}(l)]. \quad (4)$$

$G_l^\pm(\chi)$ are derived from Legendre polynomials $P_l(\chi)$ and averaged over angular bins. In practice, the angular spectra are not pure cosmological convergence spectra, but shear spectra that include contributions from the intrinsic alignments and other terms. They may include B-mode terms, but these values are negligible at this stage of the cosmic shear analysis pipeline development.

3.3 Nonlinear Power Spectrum

At large cosmological scales, structural growth is linear and well-described by a linear matter power spectrum, without concerns about the small-scale gravitational interactions between particles. We implement this linear power spectrum in our model with the Boltzmann code CAMB (Lewis et al. 2000) as applied in CosmoSIS (Zuntz et al. 2015). Smaller scales require a non-linear matter power spectrum. Currently, we are using the HaloFit model (Takahashi et al. 2012) for the non-linear matter power spectrum, but future pipeline iterations will test the impact of the HMCode (Mead et al. 2015) model.

3.4 Intrinsic Alignments

As astrophysical bodies, galaxies are not perfect or ideal tracers of underlying matter fields. They experience local gravitational interactions and environmental effects that can alter their shape. The observed shape of a galaxy can be broken into two components: the shear caused by gravitational lensing (G) and the shape induced by the local environment (I), described as $\gamma = \gamma^G + \gamma^I$. The phrase *intrinsic alignment* (IA) describes both intrinsic shape - intrinsic shape correlations between physically close galaxies (II) and shear-intrinsic correlations between galaxies on nearby lines of sight (GI). Unfortunately, the intrinsic alignment terms contribute to the total shear signal at similar angular scales as the cosmic shear, presenting a significant systematic for weak lensing analyses. As a result, we usually forward-model intrinsic alignment effects. Intrinsic alignments contribute to the E-mode angular power spectrum as follows:

$$C_{\gamma,EE}^{ij}(l) = C_{GG}^{ij}(l) + C_{GI}^{ij}(l) + C_{IG}^{ij}(l) + C_{II,EE}^{ij}(l). \quad (5)$$

The intrinsic alignment power spectra are given as:

$$C_{GI}^{ij}(l) = \int_0^{\chi_H} \frac{W^i(\chi)n^j(\chi)}{\chi^2}P_{GI}(\frac{l+1/2}{\chi}, z(\chi))d\chi, \quad (6)$$

and

$$C_{II}^{ij}(l) = \int_0^{\chi_H} \frac{n^i(\chi)n^j(\chi)}{\chi^2}P_{II}(\frac{l+1/2}{\chi}, z(\chi))d\chi. \quad (7)$$

We describe the models used for the intrinsic alignment power spectrum in the following two sections.

3.4.1 NLA

Typically, we assume that the the intrinsic alignments, or the correlated component of galaxy shapes, are dependent on the large-scale cosmological tidal field. "Tidal alignment" thus describes the impact of tidal gravitational forces from the surrounding environment on galaxy shapes. We can link the shape component to the gravitational potential at the time of galaxy formation ϕ,

$$(\gamma_1^I, \gamma_2^I) = A_1(z)(\frac{\delta^2}{\delta x^2} - \frac{\delta^2}{\delta y^2}, 2\frac{\delta^2}{\delta x\delta y})\phi_*. \quad (8)$$

γ stands for the shear. $A_1(z)$, the main parameter used to model the intrinsic alignment process, encapsulates the response of the intrinsic shape to the tidal field. The popular Nonlinear Alignment Model (NLA, Bridle & King 2007; Hirata et al. 2007) uses the nonlinear, small-scale tidal field to calculate the tidal alignment term as

$$A_1(z) = -a_1\bar{C}_1\frac{\rho_{\rm crit}\Omega_m}{D(z)}(\frac{1+z}{1+z_0})_1^\eta. \quad (9)$$

$D(z)$ is the linear growth factor, $\rho_{\rm crit}$ is the critical density, a_1 is a dimensionless amplitude, z_0 is a pivot redshift, η_1 is a power law index, and $\bar{C}_1$ is a normalization constant. a_1 and η are free parameters in the cosmological model. Under the NLA model, the GI and II power spectra are modified only by the $A_1(z)$ term:

$$P_{GI}(k,z) = A_1(z)P_\delta(k,z), \quad (10)$$

$$P_{II}(k,z) = A_I^2(z)P_\delta(k,z). \quad (11)$$

3.4.2 TATT

More complex and generalized alignment processes can be described by the Tidal Alignment and Tidal Torquing (TATT, Blazek et al. 2019) framework. Tidal torquing focuses on how the tidal field from the surrounding environment affects the rotation of galaxies. TATT expands the matter density field δ and the tidal field s_{ij} as

$$\gamma_{ij}^{IA} = A_1 s_{ij} + A_{1\delta}\delta s_{ij} + A_2 \Sigma_k s_{ik} s_{kj} + ... \quad (12)$$

Three parameters correspond to the responses to large-scale tidal fields: A_1, A_2, and $A_{1,\delta}$. A_1 represents a linear response to the tidal field (tidal alignment), A_2 corresponds to a quadratic response (tidal torquing), and $A_{1,\delta}$ stands for the response to the product of the density and tidal fields. In this case, the GI and II power spectra will be defined as:

$$P_{GI}(k) = A_1 P_\delta(k) + A_{1\delta} P_{0|0E}(k) + A_2 P_{0|E2}(k), \quad (13)$$

$$\begin{aligned} P_{II}(k) &= A_I^2 P_\delta(k) + 2A_1 A_{1\delta} P_{0|0E} + A_{1\delta}^2 P_{0E|0E}(k) \\ &+ A_2^2 P_{E2|E2}(k) + 2A_1 A_2 P_{0|E2}(k) + 2A_{1\delta} A_2 P_{0E|E2}(k). \end{aligned} \quad (14)$$

$A_2(z)$ follows a similar definition to $A_1(z)$, with

$$A_2(z) = 5 a_2 \bar{C}_1 \frac{\rho_{\rm crit}\Omega_m}{D(z)} \left(\frac{1+z}{1+z_0}\right)^{\frac{\eta}{2}}. \quad (15)$$

The leading coefficient (5 in Eq. 15) determines the difference in the variance produced by the tidal alignment and tidal torquing power spectra. We define the $A_{1\delta}$ factor as $A_{1\delta} = b_{TA} A_1$, where b_{TA} is the linear bias of source galaxies contributing to the tidal alignment signal. In total, the TATT model marginalizes over five parameters, $(a_1, a_2, \eta_1, \eta_2, b_{\rm TA})$, leading to increased flexibility and a better capture of intrinsic alignment behavior. Despite these advantages, Secco et al. (2022) found that DES didn't show a preference for TATT over NLA. The DES data quality was not high enough to utilize the power and flexibility of TATT to reduce bias. Given that DELVE has similar data quality to DES, we will likely run into similar problems. Thus, we base our fiducial pipeline around the NLA model. We include comparisons between the NLA and TATT frameworks in Sec. 4.3.1.

3.5 Scale Cuts

The impact of baryons on the matter power spectrum at cosmological scales represents another source of significant uncertainty. For example, feedback processes from AGN and supernovae may heat their environments and suppress matter clustering, while metal enrichment may offer cooling channels that increase small-scale clustering. To avoid these uncertainties, we remove the most heavily impacted angular scales from the data vector. We determine these scale cuts by first constructing a synthetic data vector "contaminated" by baryonic processes. We overview the process for building a synthetic data vector in Sec. 3.1. To produce the contaminated data vector, we apply the OWLS-AGN (van Daalen et al. 2011) matter power spectrum, which represents one of the most extreme AGN-feedback scenarios in literature. Next, we calculate the $\Delta\chi^2$ between the contaminated data vector and an uncontaminated, synthetic baseline vector. We progressively remove angular scales until $\Delta\chi^2 < 0.3$, representing a 0.3σ difference between the contaminated and uncontaminated vectors. We present a visualization of the scale cuts in Fig. 1. We note that the ξ_- shear measurements (bottom right triangle) are more heavily affected by baryon contamination and thus require more intensive scale cuts.

3.6 Nuisance Parameters

Outside of the cosmological and intrinisc alignment free parameters, several nuisance parameters can be incorporated into cosmic shear analyses to absorb additional sources of uncertainty. One such example is the redshift distribution uncertainty, which we parameterize as a uniform shift in the mean of the redshift distribution. Other examples include the uncertainty surrounding shape calibration and its response to blending, which we usually characterize as a rescaling of the two-point correlation prediction. At this point in pipeline development, we have fixed the nuisance parameters to produce a more conservative constraint.

4 COSMOLOGY FORECASTS

In this section, we overview the priors and the marginalization process used to forecast the cosmological constraints and compare the impact of various modeling choices on the posteriors. We also include a comparison between the predicted DELVE results and the DES Y3 constraints. We emphasize that these plots are projections and shown as a check on the success of the pipeline.

4.1 Parameter Inference

To extract the forecast parameter constraints, we must fit the theoretical shear model to the synthetic data vector using Bayesian posterior estimation. We assume that the likelihood of the data given a model M with parameters p will follow a multivariate Gaussian,

$$\ln \mathcal{L}(\mathbf{D}|\mathbf{p}, M) = -\frac{1}{2}\chi^2 \quad (16)$$

$$\chi^2 = (\mathbf{D} - \mathbf{T}_M(\mathbf{p}))^T \mathbf{C}^{-1} (\mathbf{D} - \mathbf{T}_M(\mathbf{p})). \quad (17)$$

$\mathbf{C}$ represents the data covariance matrix and $\mathbf{T}_M(\mathbf{p})$ stands for the predicted theory vector for a data vector $\mathbf{D}$, given the parameters $\mathbf{p}$. The *Bayes Theorem* transforms the likelihood function into $P(\mathbf{p}|\mathbf{D}, M)$, or the probability that the parameters $\mathbf{p}$ take on certain values given a set of measurements $\mathbf{D}$:

$$P(\mathbf{p}|\mathbf{D}, M) = \frac{\mathcal{L}(\mathbf{D}|\mathbf{p}, M)\Pi(\mathbf{p}|M)}{P(\mathbf{D}|M)}, \quad (18)$$

where $\Pi(\mathbf{p}|M)$ represents the prior and $P(\mathbf{D}|M)$ signifies the evidence of the data. We sample the posterior using Nautilus (Lange 2023), a Python package that uses importance sampling and efficient space exploration with neural networks.

4.2 Priors

We summarize the priors for the cosmological and intrinsic alignment parameters in Tab. 2. For our fiducial analysis, we fix the nuisance parameters, including the shear bias and photo-z errors, and select the NLA intrinsic alignment framework. We include comparisons to TATT in Sec. 4.3.1.

4.3 Modeling Choices

We compare the impact of different modeling choices on the posteriors of the cosmological constraints for the DELVE pipeline. We focus on two major choices: the intrinsic alignment model, and the use of scale cuts to mitigate baryon contamination.

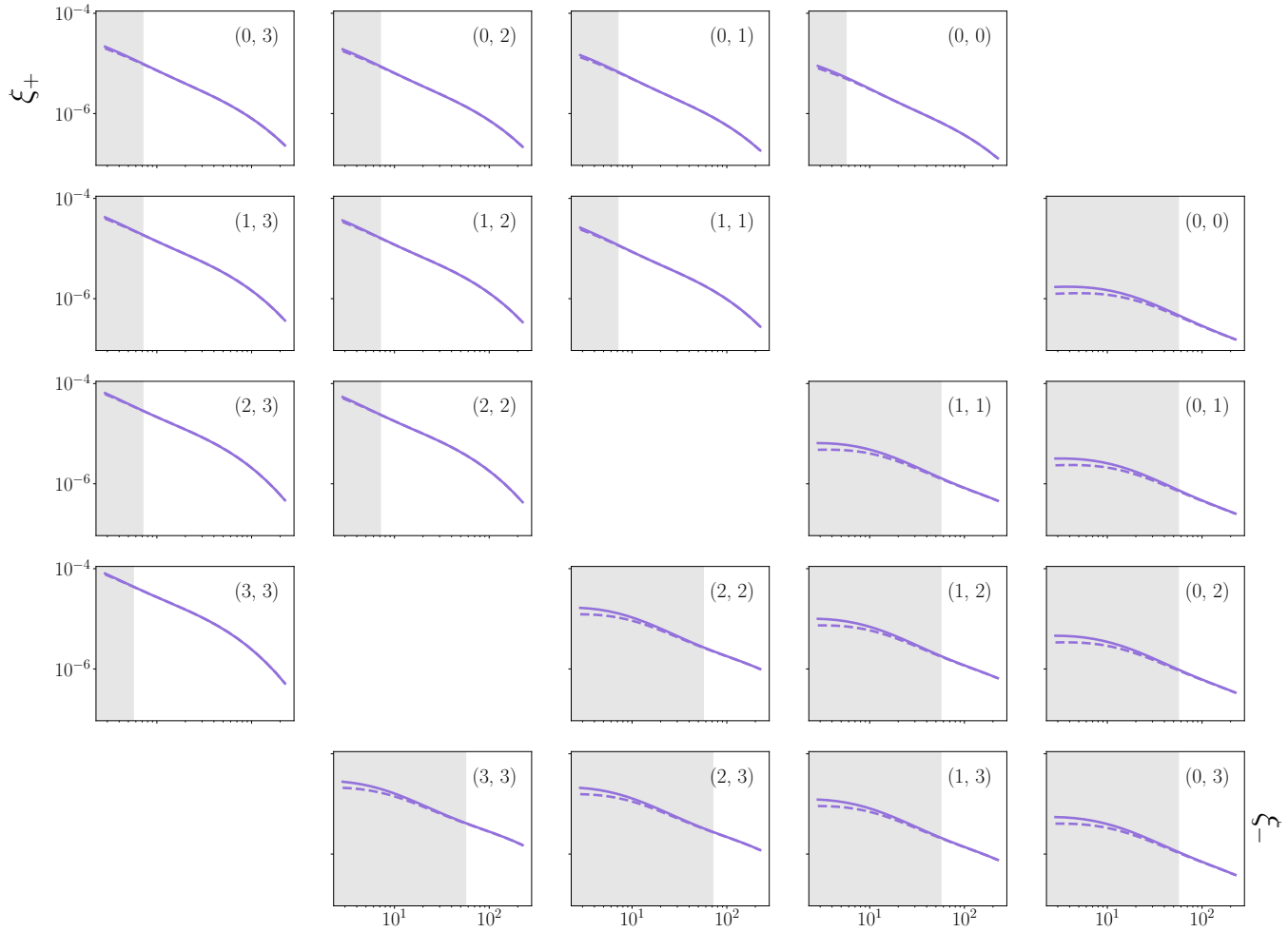

Figure 1. Scale cuts (gray shading) compared to fiducial, uncontaminated data vector (solid line) and contaminated data vector (dashed line) for each tomographic bin combination. The upper left triangle represents the ξ_+ correlation measurements and the bottom right triangle represents the ξ_- correlation measurements. The ξ_- measurements are more heavily impacted by the scale cuts.

Parameter	Prior
Cosmological Parameters	
Ω_m	U[0.1, 0.9]
h	U[0.55,0.91]
Ω_b	U[0.03, 0.07]
N_s	U[0.87, 1.07]
A_s	U[0.5, 5] $\times 10^{-9}$
$\Omega_\nu h^2$	U[0.6, 6.44] $\times 10^{-3}$
Intrinsic Alignment Parameters	
a_1	U[-5,5]
η_1	U[-5,5]

Table 2: A summary of the priors used in the fiducial analysis. The top six rows are cosmological parameters, while the bottom section represents the intrinsic alignment parameters. We note that these priors correspond to the NLA intrinsic alignment framework, and the TATT framework requires additional parameters.

4.3.1 NLA vs. TATT

We compare the impact between selecting the NLA model or the TATT model on the posteriors. As previously mentioned, we use the NLA model for our fiducial pipeline. NLA requires only one additional systematics parameter, thus it produces tighter constraints than TATT. TATT's inclusion of tidal torquing improves modeling flexibility, but the framework is overly conservative for the DELVE data quality and produces larger errorbars without reducing bias. We show both the TATT and NLA parameterization separately in Fig. 2 and Fig. 3, and present the comparison in Fig. 4. The NLA model is biased towards slightly higher values of Ω_m and S_8 and is slightly more constrained than the TATT model. Including scale cuts deepens this effect, as shown in Sec. 4.3.2.

4.3.2 Scale Cut Impact

In this section, we show the impact of baryon contamination and scale cuts on the posteriors for the cosmological parameter constraints. In Fig. 5, we demonstrate the effects of baryon contamination on data vectors. Regardless of the intrinsic alignment framework, baryon contamination significantly offsets the S_8 posterior. Applying scale cuts mitigates the impact of baryon contamination, as shown in Fig 6.

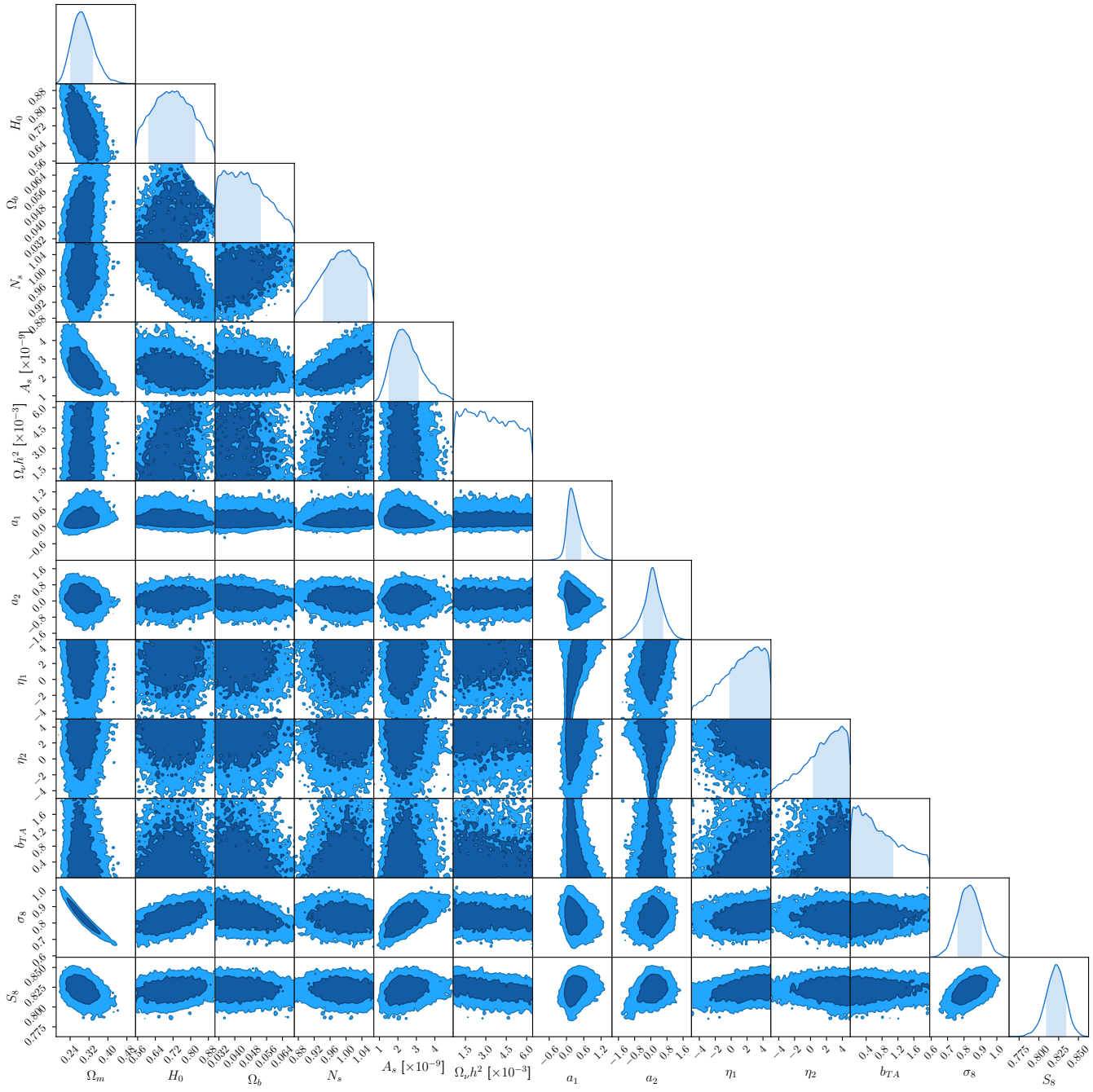

Figure 2. Posterior for the cosmological parameters and intrinsic alignment parameters for an uncontaminated data vector using the TATT intrinsic alignment model without scale cuts. Ω_m represents the matter density of the Universe and H_0 is the current expansion rate of the Universe with units of $\frac{\text{km}}{\text{Mpc s}}$. Ω_b stands for the baryonic matter density of the Universe. N_s represents the scalar spectral index and A_s is the amplitude of the primordial scalar fluctuations. $\Omega_\nu h^2$ is the fractional energy density of neutrinos in the Universe. a_1 is the amplitude of the tidal alignment signal and a_2 is the amplitude of tidal torquing. η_1 and η_2 are power law indices. b_{TA} represents the linear bias of source galaxies contributing to the tidal alignment signal. σ_8 characterizes the amplitude of matter density fluctuations at 8 Mpc. S_8 is the amplitude of clustering at 8 Mpc and is usually expressed with units of Mpc.

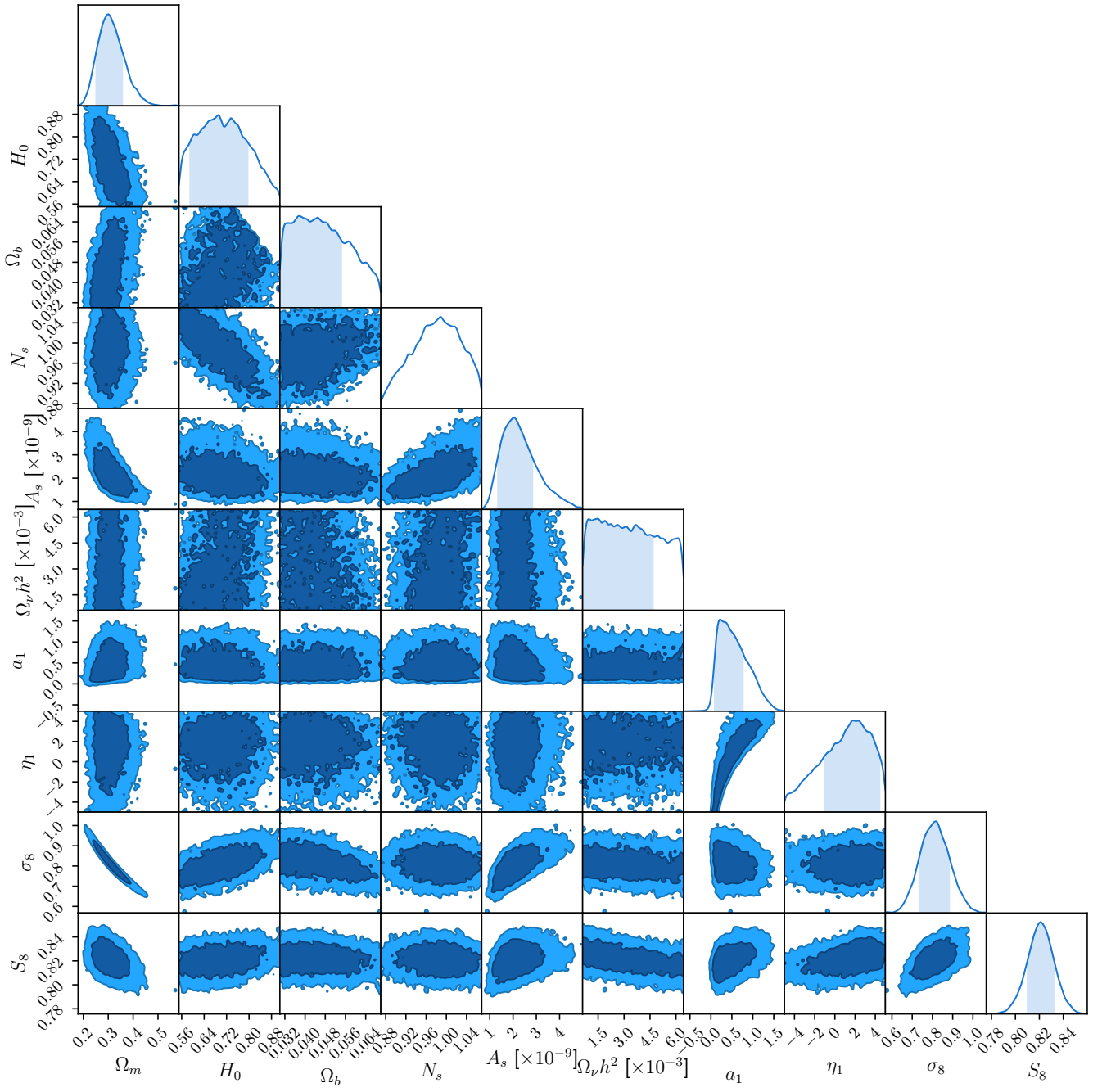

Figure 3. Posterior for the cosmological parameters and intrinsic alignment parameters for an uncontaminated data vector using the NLA intrinsic alignment model without scale cuts. Ω_m represents the matter density of the Universe and H_0 is the current expansion rate of the Universe with units of $\frac{\text{km}}{\text{Mpc s}}$. Ω_b stands for the baryonic matter density of the Universe. N_s represents the scalar spectral index and A_s is the amplitude of the primordial scalar fluctuations. $\Omega_\nu h^2$ is the fractional energy density of neutrinos in the Universe. a_1 is the amplitude of the tidal alignment signal and η_1 is the power law index. σ_8 characterizes the amplitude of matter density fluctuations at 8 Mpc. S_8 is the amplitude of clustering at 8 Mpc and is usually expressed with units of Mpc.

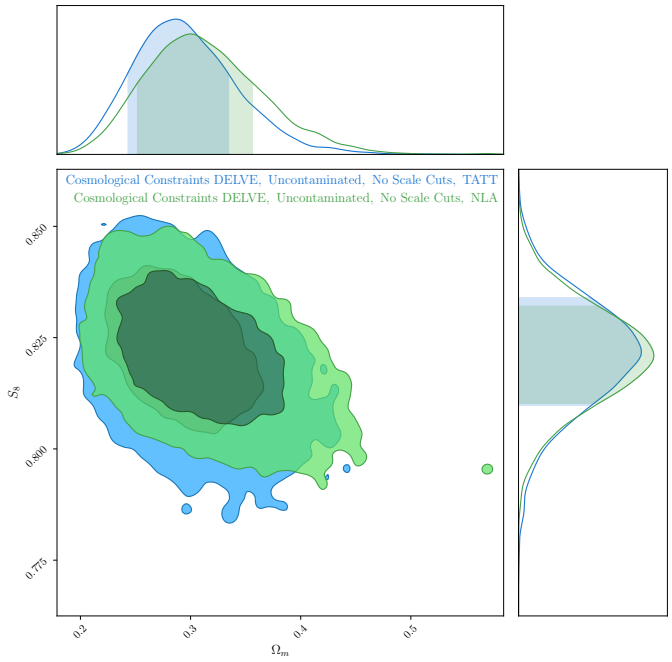

Figure 4. Posterior comparing the Ω_m and S_8 terms between uncontaminated data vectors with no scale cuts and NLA and TATT intrinisc alignment models.

These scale cuts reduce the offset and create a model that produces consistent results regardless of the environment. Our current working fiducial pipeline thus uses the NLA intrinsic alignment framework and includes both scale cuts and baryon contamination.

4.4 Comparison to DES Year 3

In this section, we compare the projected constraining power of our current pipeline to the DES Year 3 cosmic shear analysis results. DES covers approximately $\sim 4100\,\mathrm{deg}^2$ of the sky with 100 million galaxies, while DELVE observations span $\sim 5500\mathrm{deg}^2$ with 107 million galaxies, resulting in a shallower survey and lower galaxy number density. We note that the DES fiducial model uses a different starting cosmology (described in Secco et al. 2022), thus our results will be artificially offset. Furthermore, DES uses the TATT rather than the NLA model, causing a broader posterior distribution. Nonetheless, we find that the projected DELVE fiducial cosmic shear pipeline possesses equivalent constraining power to DES, boding well for the full analysis. We compare the DELVE posterior for the Ω_m and S_8 term using both the NLA and TATT intrinsic alignment frameworks to the DES posterior in Fig. 7.

5 CONCLUSIONS

We develop the pipeline for cosmic shear analysis and forecast cosmological constraints for the DELVE survey. We produce simulated cosmic shear data vectors using the theoretical shear model, fix nuisance parameters, test the impact of different intrinsic alignment models, and construct and apply scale cuts to mitigate the effects of baryon contamination. The resulting pipeline projects cosmological constraints that are comparable in power to the DES Y3 cosmic shear analysis. This pipeline will prove crucial to the full DELVE cosmic shear analysis, which will both independently cross-check

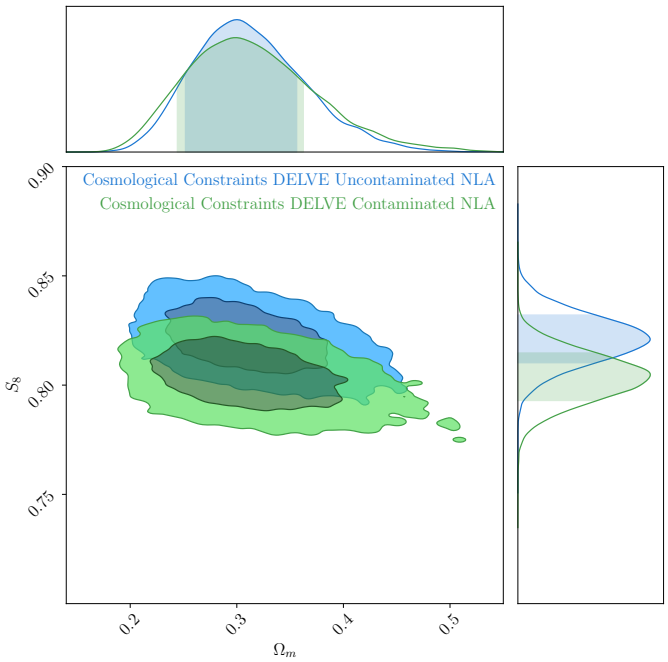

(a) NLA IA

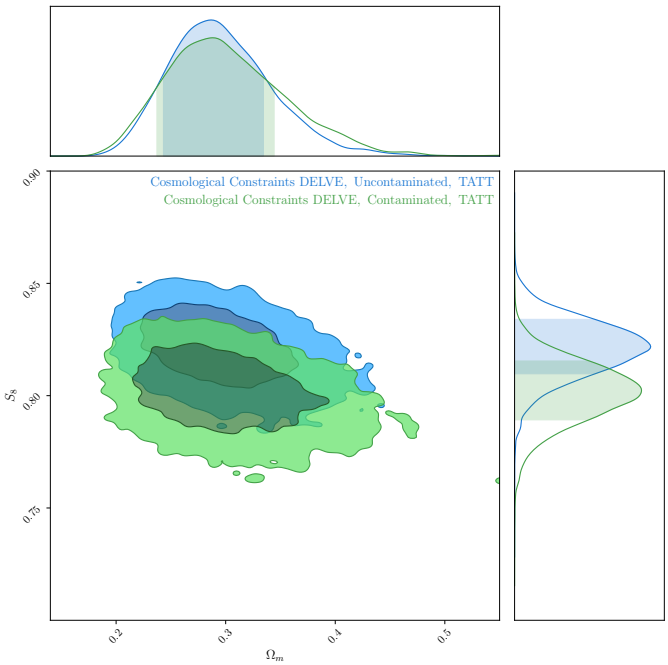

(b) TATT IA

Figure 5. Posterior comparing the Ω_m and S_8 terms between uncontaminated and contaminated data vectors with no scale cuts for both NLA (top) and TATT (bottom) intrinisc alignment models.

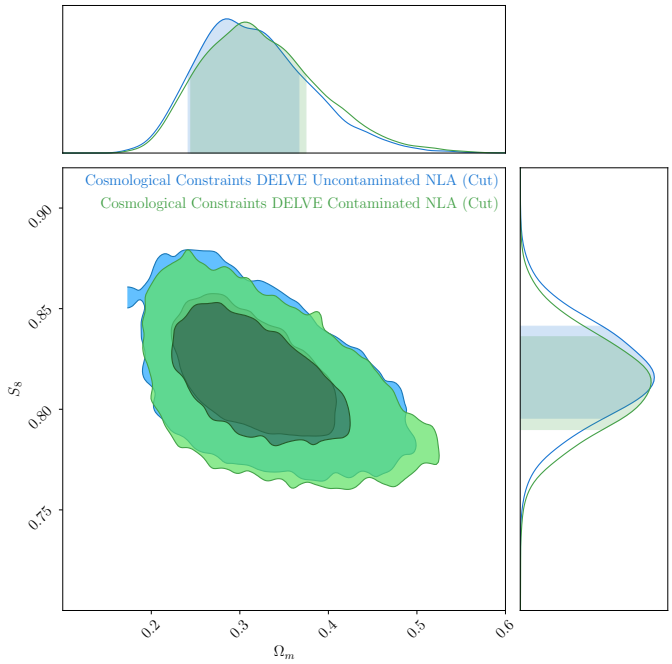

(a) NLA IA

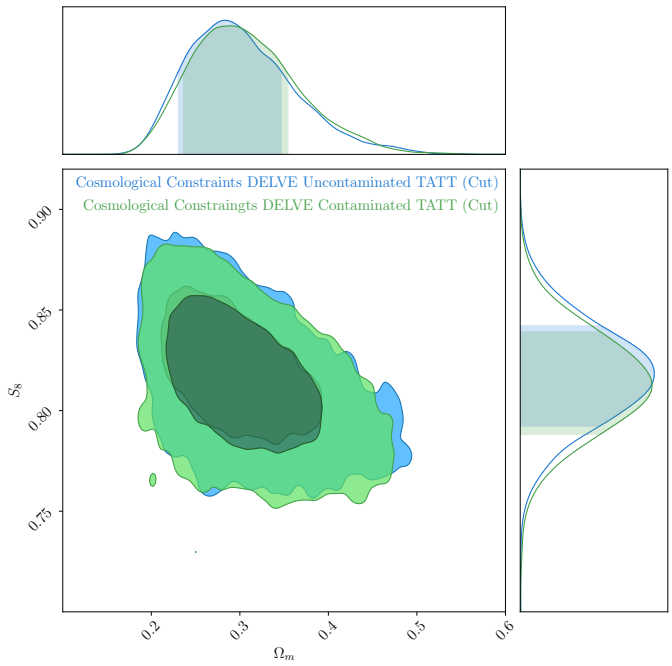

(b) TATT IA

Figure 6. Posterior comparing the Ω_m and S_8 terms between uncontaminated and contaminated data vectors with applied scale cuts for both NLA (top) and TATT (bottom) intrinsic alignment models.

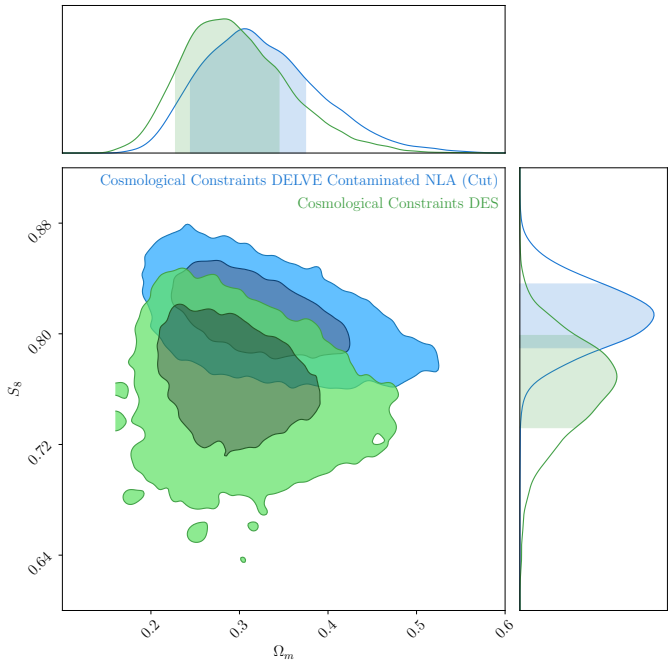

(a) DELVE (NLA) vs. DES

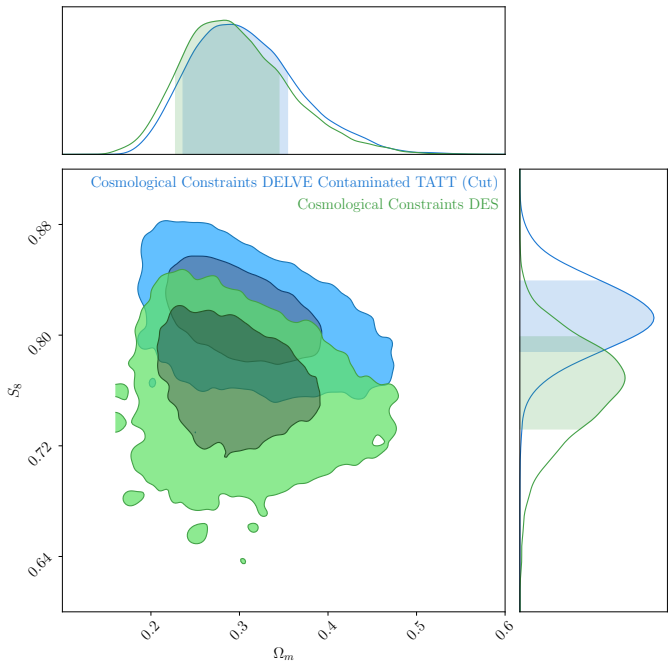

(b) DELVE (TATT) vs. DES

Figure 7. Posterior comparing the Ω_m and S_8 terms between the DELVE posteriors (NLA top, TATT bottom) and the DES posteriors.

the DES cosmic shear analysis and, when combined with DES, potentially increase the constraining power on S_8. These improvements will lead to a better grasp of the ΛCDM model and a deeper understanding of whether the S_8 tension is a sign of new physics or points to a need for improved systematic analysis. Currently, more DELVE data is undergoing analysis. The next steps for this project will include evaluating the nonlinear matter power spectrum modeling, understanding the impact of shear ratios on the DES constraints, and testing the pipeline results using the cosmic shear measurements from the final DELVE shear catalog.

ACKNOWLEDGMENTS

This work was supported in part by the U.S. Department of Energy, Office of Science, Office of Workforce Development for Teachers and Scientists (WDTS) under the Science Undergraduate Laboratory Internships Program (SULI).

REFERENCES

Abbott T. M. C., et al. 2018, Phys. Rev. D, 98, 043526
Aihara H., et al. 2018, PASJ, 70, S4
Amon A., et al. 2022, Phys. Rev. D, 105, 023514
Asgari M., et al. 2021, A&A, 645, A104
Bassett B., Hlozek R., 2010, in Ruiz-Lapuente P., ed., , Dark Energy: Observational and Theoretical Approaches. p. 246, doi:10.48550/arXiv.0910.5224
Blazek J. A., et al. 2019, Phys. Rev. D, 100, 103506
Bridle S., King L., 2007, New Journal of Physics, 9, 444
Dark Energy Survey Collaboration 2016, MNRAS, 460, 1270
Drlica-Wagner A., et al. 2021, ApJS, 256, 2
Durrer R., 2015, Classical and Quantum Gravity, 32, 124007
Flaugher B., et al. 2015, AJ, 150, 150
Hikage C., et al. 2019, PASJ, 71, 43
Hirata C. M., et al. 2007, MNRAS, 381, 1197
Lange J. U., 2023, MNRAS, 525, 3181
Lewis A., Challinor A., Lasenby A., 2000, ApJ, 538, 473
Mead A. J., et al. 2015, MNRAS, 454, 1958
Natarajan P., et al. 2024, Space Sci. Rev., 220, 19
Planck Collaboration 2020, A&A, 641, A6
Secco L. F., et al. 2022, Phys. Rev. D, 105, 023515
Takahashi R., et al. 2012, ApJ, 761, 152
Zuntz J., et al. 2015, Astronomy and Computing, 12, 45
de Jong J. T. A., et al. 2013, Experimental Astronomy, 35, 25
van Daalen M. P., et al. 2011, MNRAS, 415, 3649